

# Parametric Oscillation with Wineglass Disk Resonators

*Thanh-Phong Nguyen  
Clark Nguyen, Ed.*



Electrical Engineering and Computer Sciences  
University of California at Berkeley

Technical Report No. UCB/EECS-2018-179

<http://www2.eecs.berkeley.edu/Pubs/TechRpts/2018/EECS-2018-179.html>

December 14, 2018

Copyright © 2018, by the author(s).  
All rights reserved.

Permission to make digital or hard copies of all or part of this work for personal or classroom use is granted without fee provided that copies are not made or distributed for profit or commercial advantage and that copies bear this notice and the full citation on the first page. To copy otherwise, to republish, to post on servers or to redistribute to lists, requires prior specific permission.

# Parametric Oscillation with Wineglass Disk Resonators

by Thanh-Phong Nguyen

## Research Project

Submitted to the Department of Electrical Engineering and Computer Sciences, University of California at Berkeley, in partial satisfaction of the requirements for the degree of **Master of Science, Plan II**.

Approval for the Report and Comprehensive Examination:

Committee:

Professor Clark T.C. Nguyen

Research Advisor

(Date)

\* \* \* \* \*

Professor Bernhard E. Boser

Second Reader

(Date)

## **Abstract**

Parametric oscillation provides another avenue to excite micro electro-mechanical resonators into oscillation. Rather than driving the resonator at its resonant frequency, modulating the stiffness of the resonator forces this motion. While this technique can lead to failures, it also can provide methods for frequency division, phase noise reduction, and sustaining oscillations of various frequency with a single amplifier. This work models the voltage conditions for parametric oscillation and compares them to measured results with an accuracy of 15%. Discrepancies caused by assumptions of the driving signal and measurement noise cause the difference between the theoretical and experimental results. Additionally, this work characterizes the frequency conditions for parametric oscillation. By sweeping the frequency from high to low and low to high, the driving frequencies that cause parametric oscillation are determined. This work also investigates a shorting failure mode caused by a large driving signal that decreases the quality factor of the device.

## **Acknowledgements**

I would like to express my gratitude to my professor, Clark Nguyen, for his guidance in research and for being a great example of a teacher.

I would also like to thank Professor Bernhard Boser for being the second reader of this report and giving me the opportunity to teach a very interesting and rewarding class.

Additionally, I am thankful to my group members. To Ruonan Liu and Jalal Nilchi for their guidance in measuring resonators. To Zeying Ren and Alper Ozgurluk for fabricating the resonators that this work is based on. And to Alain Antón, Kieran Peleaux, Qianyi Xie, Kyle Tanghe, Gleb Melnikov, and Yafei Li for their help and support throughout the years. Special thanks goes to Alain Antón, Kieran Peleaux, Qianyi Xie, and Kyle Tanghe for being great friends inside and outside of the lab.

Lastly, I would like to thank my family and friends for their unwavering support through the last two and a half years.

# 1 TABLE OF CONTENTS

---

2	Introduction .....	1
2.1	Background and Objective .....	1
3	Conditions for Parametric Oscillation .....	2
3.1	Theory of Operation.....	2
3.2	Experimental Procedure .....	5
3.3	Experimental Results .....	6
3.3.1	Resonators .....	6
3.3.2	Voltage Conditions.....	9
3.3.3	Frequency Conditions .....	12
3.3.4	Stability and Safety .....	15
4	Conclusion.....	19
4.1	Results.....	19
4.2	Future Research .....	20
5	References .....	21

## 2 INTRODUCTION

### 2.1 BACKGROUND AND OBJECTIVE

Resonators generally only react to inputs that are close to its resonant frequency. However, a well-known phenomenon called parametric oscillation can cause a resonator to oscillate when driven by a frequency far from its resonant frequency. Essentially, if the resonator has a modulated mechanical property at twice the resonant frequency of the device, then oscillations can occur. In this work, a time varying biasing voltage applied to the resonator modulates its stiffness. The changing capacitance converts the time varying voltage into a time varying electrical stiffness. If this change in stiffness is large enough, oscillations will occur. The parametric driving voltage does not actually create any forces on the disk due to being far from the resonant frequency. This phenomenon has been proved as far back as 1887 and demonstrated by various research efforts [1] [2] [3]. However, the conditions for parametric oscillation for capacitively transduced wineglass disk resonators has not been explicitly stated. This work aims to prove and demonstrate the conditions for parametric oscillation for wineglass disk resonators.

Potential applications of such a technique include frequency dividers for phase-locked loops, frequency synthesizers, and filters. Capacitively transduced micromechanical wineglass disk resonators have proven to parametrically oscillate and even reduce the phase noise of the input signal [2]. By understanding the conditions of parametric oscillation, multiple resonators can be daisy-chained together in order to reduce the phase noise even further. This technique requires frequency matching among the devices and is not the focus of this work due to this limitation. Alternatively, daisy-chaining multiple devices could create a mechanism to generate various harmonically-related frequency terms in order to create a frequency synthesizer. Another benefit is that only one amplifier is required in both applications to sustain oscillation for the largest frequency device. Figure 2.1 demonstrates the schematic necessary for both applications.

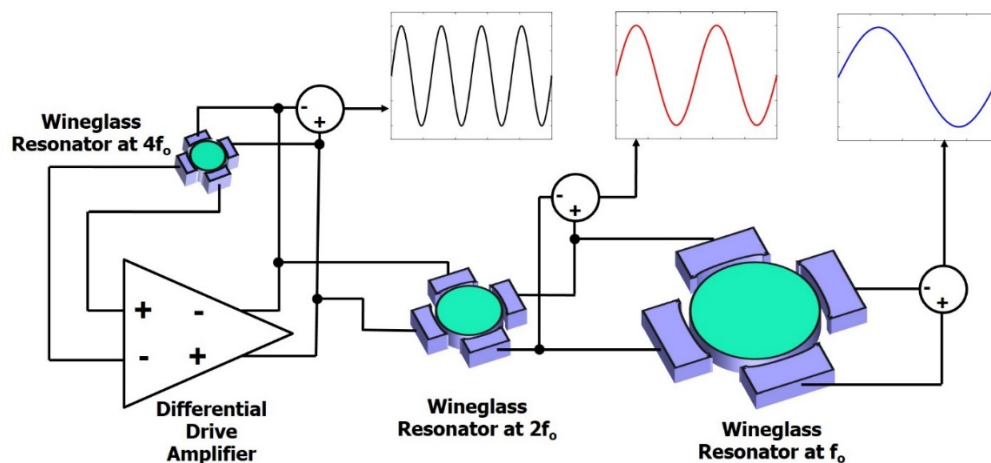


Figure 2.1. Schematic of daisy chained parametrically oscillating devices with one sustaining amplifier for phase noise reduction or frequency synthesis.

### 3 CONDITIONS FOR PARAMETRIC OSCILLATION

---

#### 3.1 THEORY OF OPERATION

Equation (3.1) describes the motion of an un-driven resonator with time varying stiffness where  $m$  is the mass,  $x$  is the position of the resonator,  $\omega_{nom}$  is the natural resonant frequency of the resonator,  $k_o$  is the mechanical stiffness of the resonator,  $Q$  is the quality factor, and  $k_e(t)$  is a time varying stiffness.

$$m \frac{d^2x}{dt^2} + \frac{m\omega_{nom}}{Q} \frac{dx}{dt} + (k_o - k_e(t))x = 0 \quad (3.1)$$

The resonators used in this work are parallel-plate capacitive-gap transduced micromechanical disk resonators. Due to the geometry of these resonators, the nonlinearity of the changing capacitive gap create an electrical stiffness [4]. If the capacitive gap voltage is time varying, the electrical stiffness will be time varying and in the form of equation (3.2), where  $C(x)$  the capacitance between the resonator disk and the electrodes and  $V_g(t)$  is the capacitive gap voltage between the disk and the electrodes.

$$k_e(t) = \frac{1}{2} \frac{\partial^2 C(x)}{\partial x^2} (V_g(t))^2 \quad (3.2)$$

The time varying biasing signal technically creates a force on the resonator. However, we will assume that the frequency of the force will be far from the resonant frequency of the resonator and the quality factor of the resonator is sufficiently large. Thus, this force is negligible [1]. The case of interest is when the gap voltage has a static component and a time varying component that is approximately twice the resonant frequency of the device. By assuming small motion and frequency terms larger than twice the resonant frequency are negligible, equation (3.2) can be approximated by equation (3.3), where  $d_o$  is the gap between the electrode and the disk,  $C_o$  is the static overlap capacitance between the electrodes and the disk,  $V_p$  is the DC gap voltage,  $V_D$  is the amplitude of the time varying gap voltage,  $\omega$  is a frequency close to the resonant frequency, and  $\kappa$  is a modifying factor that applies when there is non-uniform motion along the area of the electrodes [4]. Equation (3.3) shows that the electrical stiffness has both static and time varying components. The static electrical stiffness shifts the resonant frequency of the device from the natural mechanical resonant frequency of the disk structure. The time varying component can give rise to parametric oscillation [2].

$$k_e(t) \approx \frac{\kappa^2 C_o}{d_o^2} \left( V_p^2 + \frac{1}{2} V_D^2 \right) + 2 \frac{\kappa^2 C_o}{d_o^2} V_p V_D \cos(2\omega t) \quad (3.3)$$

Substituting equation (3.3) into (3.1), changing the unit of time, and renaming variables as dictated by Table 3.1 yields equation (3.4), also known as the linear Mathieu equation. This work uses Hill's infinite determinate with the inclusion of the damping term in order to determine the conditions for parametric oscillation [1] [5].



$$\frac{d^2x}{d\tau^2} + 2K \frac{dx}{d\tau} + (\Theta_o + 2\Theta_1 \cos 2\tau)x = 0 \quad (3.4)$$

Table 3.1. Variables List

Equation	Description
$k_{e0} = \frac{\kappa^2 C_o}{d_o^2} \left( V_p + \frac{1}{2} V_D \right)$	Static Electrical Stiffness
$k_{e2} = \frac{\kappa^2 C_o}{d_o^2} V_p V_D$	Dynamic Electrical Stiffness
$\omega_o^2 = \frac{k_e - k_{e0}}{m} = \frac{k_{tot}}{m}$	Resonant Frequency of Resonator
$\omega = \omega_o + \Delta\omega$	Driving Frequency
$\tau = \omega t$	Time Unit Change
$K = \frac{\omega_{nom}}{2\omega Q}$	Normalized Damping coefficient
$\Theta_o = \frac{1}{(1 + \Delta\omega/\omega_o)^2}$	Normalized Resonant Frequency
$\Theta_1 = -\frac{k_{e2}}{k_{tot}} \frac{1}{(1 + \Delta\omega/\omega_o)^2}$	Normalized Parametric Parameter

According to Hill, the solution of this differential equation is in the form of equation (3.5) [1]. Notice, if the normalized frequency,  $\hat{\omega}$ , is approximately equal to unity and if  $b_n = b_{-(n+1)}^*$ , then  $x(\tau)$  will be in the form of sum of cosines of the frequency  $\omega$  and its odd harmonics. We will assume that this is the case in this analysis. Additionally, we will assume that all harmonics above the third will be negligible.

$$x(\tau) = \sum_{n=-\infty}^{\infty} b_n e^{j\tau(\hat{\omega}+2n)} \quad (3.5)$$

Substituting (3.5) into (3.4) yields the system of equations (3.6). There exist nontrivial solutions to this system of equations for specific values of  $\hat{\omega}$  that make the determinant of the matrix zero. Solving for these specific frequencies yields equations (3.7)-(3.8) for the normalized frequency.

$$\begin{bmatrix} (\hat{\omega} - 2)^2 - 2jK(\hat{\omega} - 2) - \theta_o & -\theta_1 & 0 \\ -\theta_1 & \hat{\omega}^2 - 2jK\hat{\omega} - \theta_o & -\theta_1 \\ 0 & -\theta_1 & (\hat{\omega} + 2)^2 - 2jK(\hat{\omega} + 2) - \theta_o \end{bmatrix} \begin{bmatrix} b_{-1} \\ b_0 \\ b_1 \end{bmatrix} = \begin{bmatrix} 0 \\ 0 \\ 0 \end{bmatrix} \quad (3.6)$$

$$\hat{\omega} = \hat{\omega}_R + j\hat{\omega}_I = \sqrt{1 - \frac{1}{8}\theta_1 \pm B + jK} \quad (3.7)$$

$$B = \sqrt{\left(1 - \theta_o + K^2 - \frac{1}{8}\theta_1^2\right)^2 - \theta_1^2} \quad (3.8)$$

If B is imaginary, then  $\hat{\omega}$  can have a negative imaginary component, and the solution to (3.4) will be an exponentially growing sinusoid. Assuming  $\Delta\omega \ll \omega_o, Q \gg 1, k_{tot} \gg k_{e2}$ , second order powers of  $\Delta\omega/\omega_o$  are negligible, and fourth order products of  $\theta_1$  and  $K$  are negligible yields the condition for B to be imaginary and approximations for the real and imaginary components of  $\hat{\omega}$ .

$$\frac{\omega_o^2 Q^2 k_{e2}^2}{\omega_{nom}^2 k_{tot}^2} > \frac{2(1 - \theta_o)}{\theta_o(5 - \theta_o)} \approx \Delta\omega/\omega_o \quad (3.9)$$

$$\hat{\omega}_R \approx 1 + \frac{1}{32}\theta_1^2(3 - \theta_o) + \frac{1}{4}K^2(\theta_o - 1) \quad (3.10)$$

$$\hat{\omega}_I \approx K \pm \sqrt{\frac{5}{16}\theta_1^2 + \frac{1}{2}\theta_o K^2 - \frac{1}{2}K^2 - \frac{1}{16}\theta_o\theta_1^2} \quad (3.11)$$

The term  $\Delta\omega/\omega_o$  can be arbitrarily small, so B will most likely be imaginary. Substituting in values given by Table 3.1 and setting equation (3.11) less than zero yields the generic condition for parametric oscillation, equation (3.12). For most MEMS devices, the term  $\omega_o/\omega_{nom}$  is close to unity. Neglecting the  $\Delta\omega/\omega_o$  and  $\omega_o/\omega_{nom}$  terms shows that  $k_{e2}/k_{tot} > 1/Q$ , and the geometry of the resonator shows that  $k_{e2} \propto 1/d_o^2$ . Thus, the larger the quality factor of the device or the smaller the electrode-disk gap, the easier it is to create parametric oscillation. Additionally,  $k_{e2} \propto V_p V_D$ ; thus, increasing the gap voltages can induce parametric oscillation.

$$\frac{\omega_o Q k_{e2}}{2\omega_{nom} k_{tot}} > \sqrt{\frac{2(3 - \theta_o)}{\theta_o(5 - \theta_o)}} \approx 1 + \frac{5}{4} \frac{\Delta\omega}{\omega_o} \quad (3.12)$$

Substituting the values in Table 3.1 into (3.10) yields equation (3.13). From the condition of parametric oscillation,  $k_{e2}/k_{tot}$  will approximately be the same order of magnitude as  $1/Q$ . Thus, all non-unity components of  $\hat{\omega}_R$  will be proportional to  $1/Q^2$ . This work uses devices with quality factors on the

order of 10,000. Consequently, the frequency of oscillation will be essentially equal to the parametric driving frequency,  $\omega$ .

$$\hat{\omega}_R = 1 + \frac{k_{e2}^2}{16k_{tot}^2} - \frac{1}{8} \left( \frac{3k_{e2}^2}{2k_{tot}^2} + \frac{\omega_{nom}^2}{\omega_o^2 Q^2} \right) \frac{\Delta\omega}{\omega_o} \quad (3.13)$$

### 3.2 EXPERIMENTAL PROCEDURE

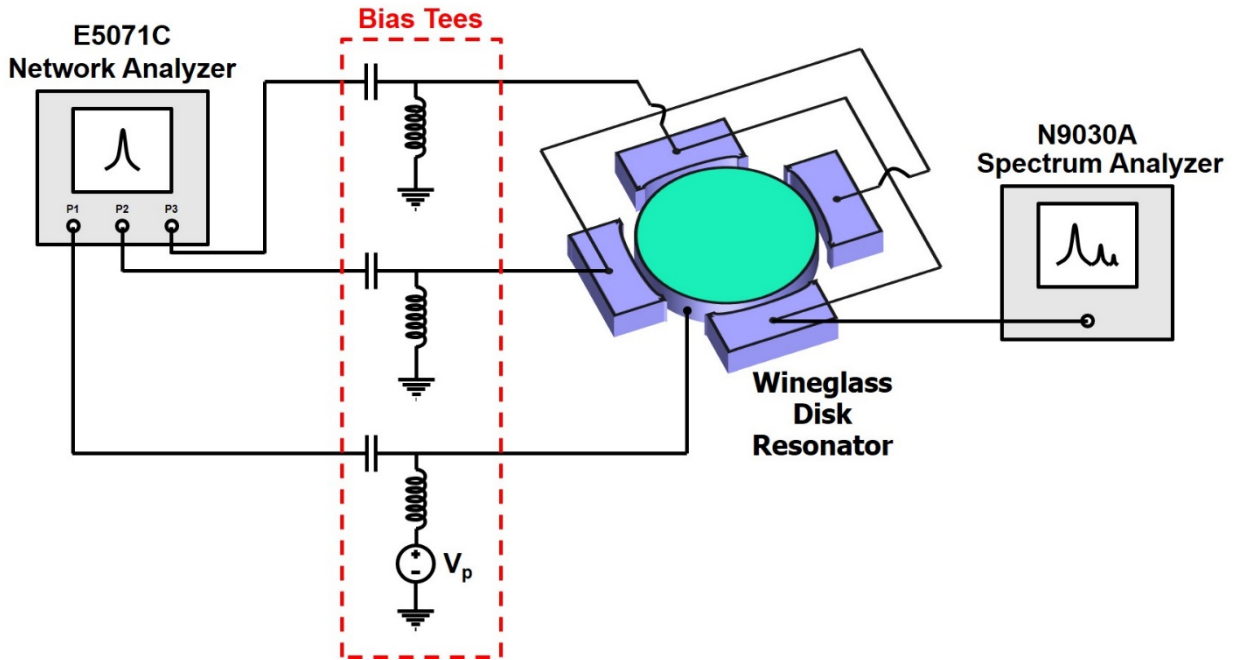


Figure 3.1. Experimental measurement setup used for all measurements in this work. The network analyzer provided the parametric drive signal and could sense the response. The spectrum analyzer could measure harmonics and the actual frequencies output by the resonators.

Figure 3.1 shows the measurement setup used for all measurements in this work. The Agilent E5071C network analyzer contains the functionality to have different drive and sense frequencies between different ports. This functionality allowed driving the disk structure or two electrodes (depending on the measurement) at frequencies approximately twice the resonant frequency and measuring signals at the other two electrodes at exactly half the driven frequency. Additionally, the E5071 has the functionality to run forwards and backwards frequency sweeps, which allows comparison to earlier works [3]. The E5071C operated in stepped mode with a 50 Hz IF bandwidth to ensure accurate measurement. The three bias tees used protect the E5071C from any DC voltages on the resonator and ensure that the DC operating points, thus the static and dynamic electrical stiffness, are controlled. The resonator itself was contained and probed in a Lakeshore model FWPX vacuum probe station capable of providing 10  $\mu$ Torr vacuum. Traces on the layout connected the electrodes of the wineglass disk resonators, so no bond wiring was required. The Agilent E3649A set the DC bias voltage,  $V_p$ .

For swept measurements, GPIB automated the testing procedure to control the E5071C and E3649A in order to sweep between different values of  $V_p$  and parametric drive voltage. The testing procedure is as follows:

1. Probe the resonator according to Figure 3.1
2. Set the current limit of the E3649A to 5 mA
3. Set the multiplier of port 1 to 2 and the multipliers of ports 2 and 3 to 1
4. Slowly ramp up the DC biasing voltage  $V_p$  to the desired value
5. Set the input power of the E5071C to approximately -30 dBm and measure the frequency response between ports 2 and 3 ( $S_{32}$ )
6. Center the frequency sweep at the resonant frequency of the resonator and set the span to approximately 10 times the bandwidth
7. Change the input power of the E5071C to correspond to the desired parametric drive voltage and measure the frequency response between ports 2 and 1 ( $S_{21}$ ).
8. Measure  $S_{21}$  with a backwards frequency sweep
9. Go to step 7 and repeat until frequency responses for all desired parametric drive voltages are measured
10. Set the input power of the E5071C to the same power as step 5 and measure  $S_{32}$
11. Go to step 4 and repeat until frequency responses for all desired  $V_p$  are measured.
12. Slowly ramp down  $V_p$  to 0 V.

For non-sweeping measurements, the N9030A measured the frequency spectrum of the response of the resonator when driven by a single frequency at a specific bias voltage and parametric drive voltage. The E5071C provided the parametric drive signal. By setting the center frequency to the desired value and setting the span to zero, the E5071C can effectively be a signal source. While not a high fidelity signal source, the E5071C was sufficient to measure the oscillating frequency of the resonator and the amplitudes of harmonics.

### 3.3 EXPERIMENTAL RESULTS

#### 3.3.1 Resonators

The data provided in this section describes the mechanical and electrical properties of the resonators used in this work. The two main resonators used in this work for parametric data are a 61MHz wineglass disk resonator fabricated by Zeying Ren in 2009 and a 13MHz wineglass disk resonator designed by Thanh-Phong Nguyen and fabricated by Alper Ozgurluk in 2018. The 61MHz wineglass disk resonator is a standard design used in many previous works [4] [2]. The 13MHz wineglass disk differs slightly from the standard design procedure in that it has a large etch hole in the center to decrease the total stiffness of the device in order to decrease the resonant frequency and to decrease the release time required for this device. A standard design for the 13MHz disk would yield a disk too large in radius to sufficiently release without negatively affecting the release of higher frequency devices on the same die. Iterative COMSOL simulations determined the inner and outer radii and mechanic stiffness of the 13MHz disk. Table 3.2 lists the various mechanical and electrical properties of each resonator. All the data marked with the asterisk are the designed values. All other values are extracted by curve-fitting measured frequency response data to appropriate models described in [4]. Note: the static overlap capacitance,  $C_{oi}$ , is for one electrode. The difference between device A and device B is that the parametric signal was applied to two electrodes for device A and applied to the disk for device B.

Table 3.2. Relevant Mechanical and Electrical Properties

Parameter	Resonator		
	61 MHz (A)	61 MHz (B)	13 MHz (C)
Outer Disk Radius, $R_{\text{disk}}$ [ $\mu\text{m}$ ]	31.4	31.4	69.0*
Outer Disk Radius, $R_{\text{hole}}$ [ $\mu\text{m}$ ]	-	-	29.2*
Nominal Frequency, $f_{\text{nom}}$ [MHz]	61.3	61.3	13.9
Electrode Span Angle, $\theta_i$ [ $^\circ$ ]	70.0*	70.0*	77.7*
Disk Thickness, $t$ [ $\mu\text{m}$ ]	3*	3*	3*
Quality Factor, $Q_o$ †	62,464	62,078	12,795
Electrode-to-resonator Gap, $d_o$ [ $\mu\text{m}$ ]	58.7	59.3	44.5
Mechanical Stiffness, $k_o$ [N/m]	$11.6 \times 10^5$	$11.6 \times 10^5$	$3.93 \times 10^5$ *
Static Overlap Capacitance, $C_{oi}$ [fF]	17.8	17.2	55.9
Varying Displacement Modifying factor, $\kappa$	0.769	0.769	0.747
Parasitic Resistance, $R_t$ [ $\Omega$ ]	287	533	312

\*Designed values

†Curve-fit value at DC bias voltage of 4V

The quality factors given are curve-fit values at 4V rather than measured values. The measured quality factor actually decreases as the DC bias voltage increases. Q-loading can explain this phenomenon [6]. Essentially, resistances on any electrode of the resonator will add extra losses and flatten out the response of the resonator with respect to frequency, thus lowering the effective quality factor. Equations (3.14)-(3.16) explain the dependence on DC bias voltage, where  $Q_o$  is the unloaded quality factor of the device,  $R_x$  is the effective electrical resistance of the resonator,  $R_t$  is any resistances on the electrodes of the device, and  $r_x$  is the motional resistance of the device. No explicit resistors are placed on the device, so  $R_t$  only includes parasitic resistances due to the traces, which should be constant with changing voltage. The motional resistance of the resonator is also constant with changing DC bias voltage. However, the effective electrical resistance decreases with the square of bias voltage. Thus, as bias voltage increases, the electrical resistance decreases, which decreases the effective quality factor. Figure 3.2 shows the measured and curve-fit values of the quality factor. All subsequent calculations used the curve-fit values of quality factor.

$$Q = Q_o \frac{R_x}{R_x + R_t} \quad (3.14)$$

$$R_x = \frac{r_x}{V_p^2 \left(\frac{\partial C}{\partial x}\right)^2} = \frac{k_o / \omega_o Q}{V_p^2 \left(\frac{\partial C}{\partial x}\right)^2} \quad (3.15)$$

$$Q = \frac{Q_o}{1 + V_p^2 \left(\frac{\partial C}{\partial x}\right)^2 \frac{\omega_o Q R_t}{k_o}} \quad (3.16)$$

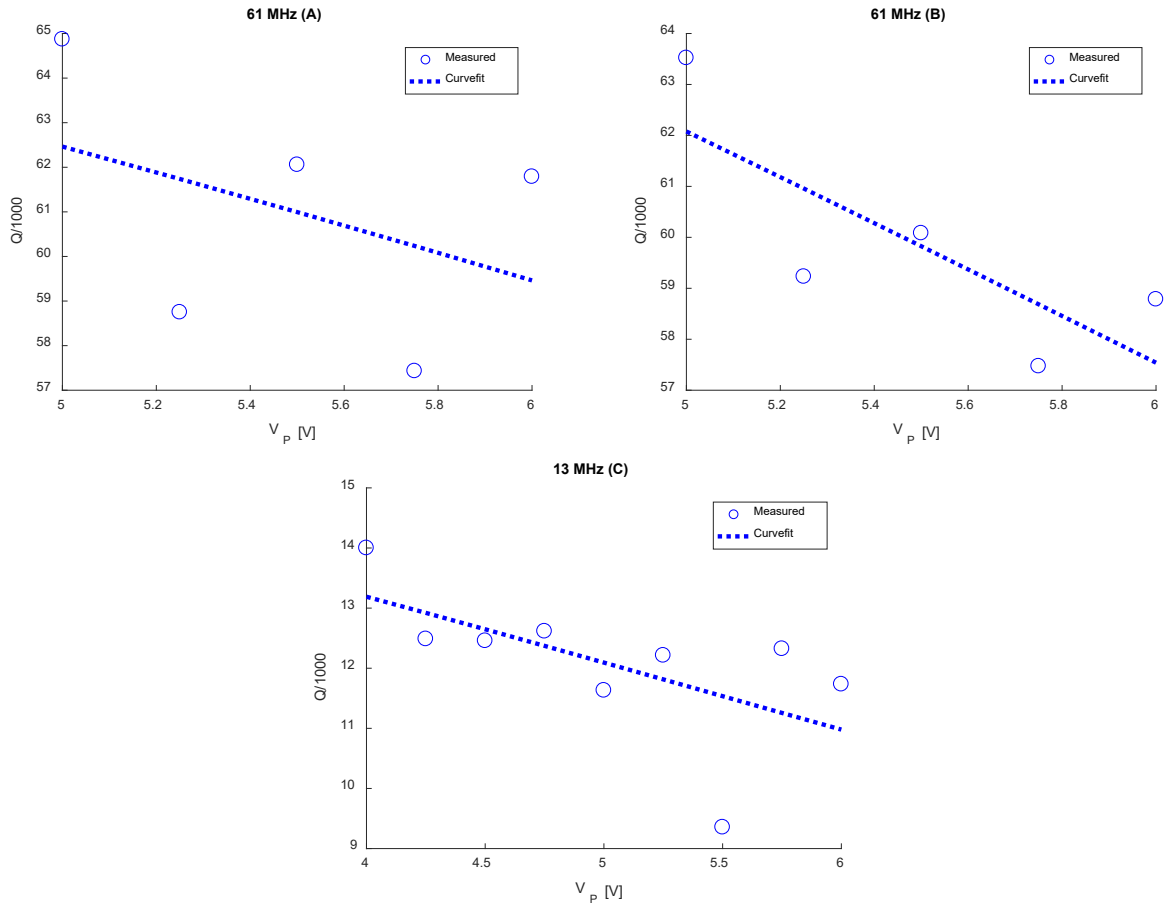


Figure 3.2. Measured and curve-fit quality factors for the three measured devices: (Top Left) Device A, (Top Right) Device B, and (Bottom) Device C.



Figure 3.3. COMSOL simulated mode shapes for (Left) 61MHz wineglass disk resonator and (Right) 13MHz wineglass disk resonator.

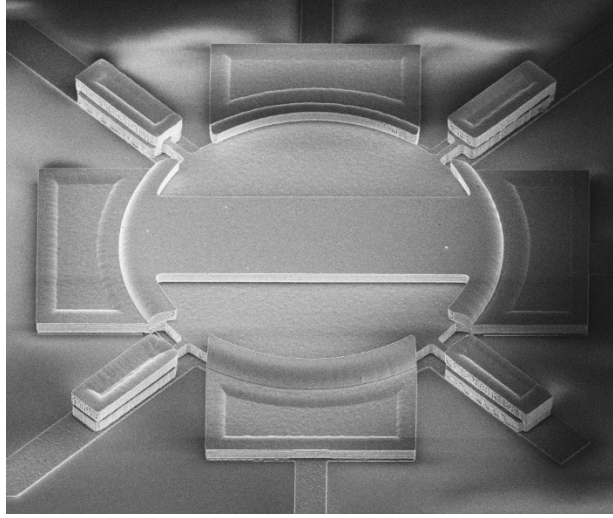


Figure 3.4. SEM of 61MHz wineglass disk resonator.

### 3.3.2 Voltage Conditions

The data provided in this section verifies the claims presented in 3.1. By substituting in values described by Table 3.1 into (3.12), assuming that the driving frequency is at resonance, and rearranging to isolate the voltage terms yields (3.17). This equation simply shows that the product of DC bias voltage and the AC bias voltage must be larger than the product of various device parameters. Technically, the terms  $\omega_o$  and  $k_{tot}$  have a dependence on  $V_p$  and  $V_D$ . However, disk resonators with gaps used in this work have low tuning capabilities [7]. Consequently, we assumed  $\omega_{nom}/\omega_o \approx 1$  and  $k_{tot} \approx k_o$  in this work. Notice:  $C_o$  is the total gap capacitance that the total capacitance that the AC bias voltage is applied across. If the AC bias voltage is applied to the disk (Port 1 in Figure 3.1), then  $C_o = 4C_{oi}$ . However, if the AC bias voltage is only applied to two electrodes (Ports 2 or 3 in Figure 3.1), then  $C_o = 2C_{oi}$ . From the theory, we would then expect that a device driven from the electrodes would require twice as much voltage than a device driven from the disk.

$$QV_pV_D > 2 \frac{\omega_{nom}}{\omega_o} k_{tot} \frac{d_o^2}{\kappa^2 C_o} \approx 2k_o \frac{d_o^2}{\kappa^2 C_o} = \Lambda \quad (3.17)$$

Table 3.3 lists the minimum drive voltages necessary for parametric oscillation and compares the measured products from (3.17). Again, devices B and C were driven parametrically from the disk, while device A was driven parametrically from two electrodes. The last column of the table shows the discrepancy between the two products; there is decent agreement with the theory. At most, there is approximately 15% error between  $\Lambda$  and  $V_pV_{D,min}Q$ . Interestingly, the error is always positive, suggesting that a lower drive voltage is necessary for parametric oscillation. The discrepancy is not due to the assumptions that  $\omega_{nom}/\omega_o \approx 1$  and  $k_{tot} \approx k_o$ , but rather come from the assumption that only harmonic terms at approximately  $2\omega_o$  are present in (3.4). Figure 3.5 shows that the drive signal has a measureable component at approximately  $4\omega_o$  and  $6\omega_o$ . The addition of these components in section 3.1 would significantly increase the complexity of the derivation by changing (3.6) into a 7x7 matrix, but could explain the decrease in expected drive voltage necessary for parametric oscillation. Another indication of the effect of the higher harmonic terms is the presence of a non-negligible harmonic term at  $3\omega_o$ . The

derivation in section 3.1 does predict a term at  $3\omega_o$ , which can be calculated by substituting (3.7) into (3.6). However, substituting measured numbers into these equations yields that the third harmonic should be >100 dB lower than the first harmonic. The measured third harmonic is actually only approximately 10 dB down from the first harmonic. Consequently, the driving terms at  $4\omega_o$  and  $6\omega_o$  are significant and can actually lower the drive voltages necessary for parametric oscillation.

Table 3.3. Measured minimum drive voltage necessary for parametric oscillation for three different wineglass disk resonators across different DC biasing voltages.

	$V_p$ [V]	$V_{D,min}$ [V]	$\Lambda$ [Nm/F]	$V_p V_{D,min} Q$ [V <sup>2</sup> ]	Error (%)
61 MHz (A)	5	1.06	379680	331612	12.7
	5.25	1.00	379682	324894	14.4
	5.5	0.946	379685	317459	16.4
	5.75	0.946	379688	327759	13.9
	6	0.946	379690	337620	11.1
61 MHz (B)	5	0.632	200375	196308	2.03
	5.25	0.564	200377	180393	9.97
	5.5	0.564	200378	185474	7.44
	5.75	0.532	200379	179569	10.4
	6	0.532	200381	183717	8.32
13 MHz (C)	4	0.238	13431	12540	6.63
	4.25	0.224	13432	12323	8.25
	4.5	0.212	13433	12058	10.2
	4.75	0.212	13434	12450	7.32
	5	0.200	13435	12094	9.98
	5.25	0.188	13436	11711	12.8
	5.5	0.188	13438	11979	10.9
	5.75	0.178	13439	11537	14.2
	6	0.178	13441	11742	12.6

Table 3.3 shows a slight increase in percent error with bias voltage for the 13 MHz (C) device. Inaccuracies in measuring the quality factor of these devices most likely cause this trend. Figure 3.6 shows the typical frequency response for device C. Even at the peak of the response, there is approximately 3 dB of noise. Rather than directly measuring the quality factor like with devices A and B, the responses of device C were fit to a Lorentz curve, and the subsequent curve was used to calculate the center frequency, bandwidth, and quality factor of the device. The designs of devices A and B are designs that consistently yield high Q devices [4] [2] [7] [8] [9]. Device C, while interesting, is not an optimized design with respect to anchor size and process. Device C was created in a process that targeted 10nm gaps. Clearly, device C does not have 10nm gaps, and the low quality factor indicates that the process and design can be further optimized.



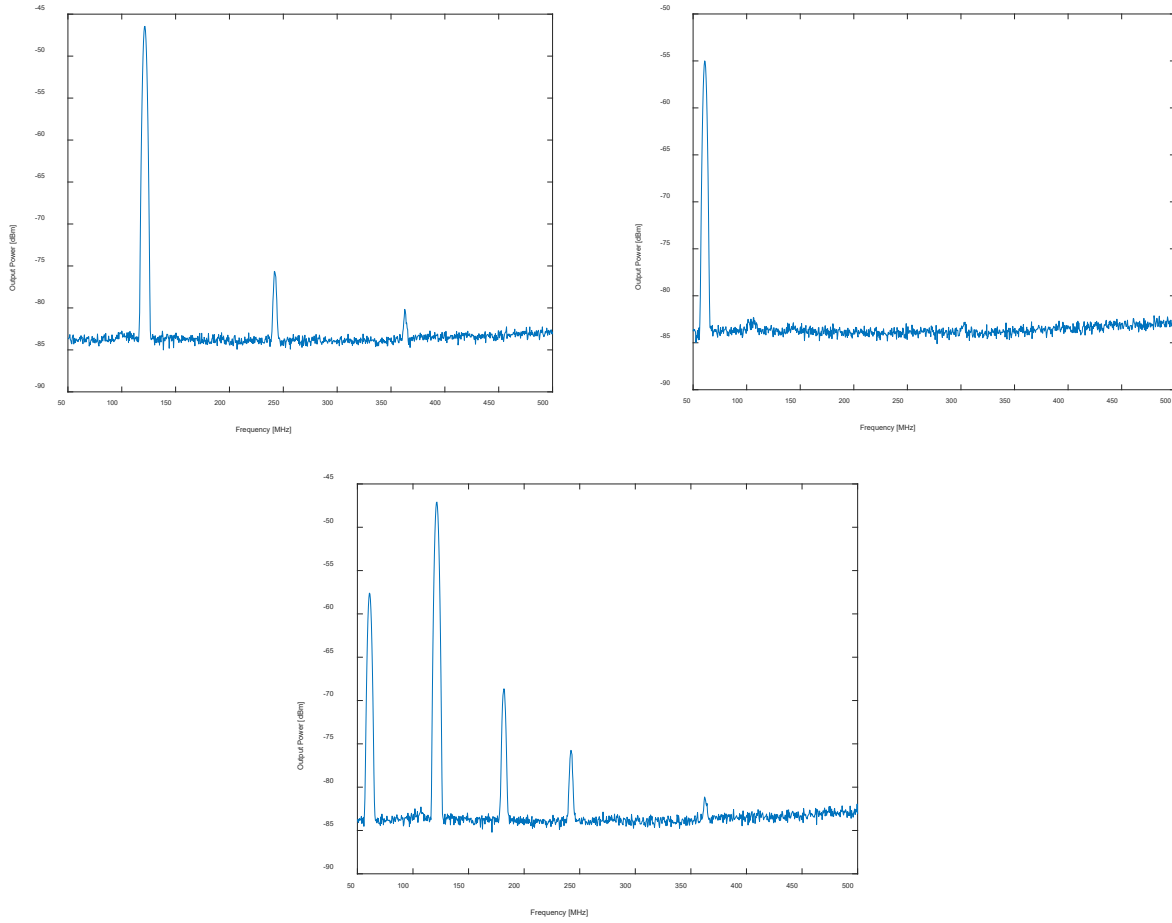


Figure 3.5. Measured harmonics of (Top Left) drive signal, (Top Right) resonator driven at resonant frequency, and (Bottom) resonator driven at twice-resonant frequency.

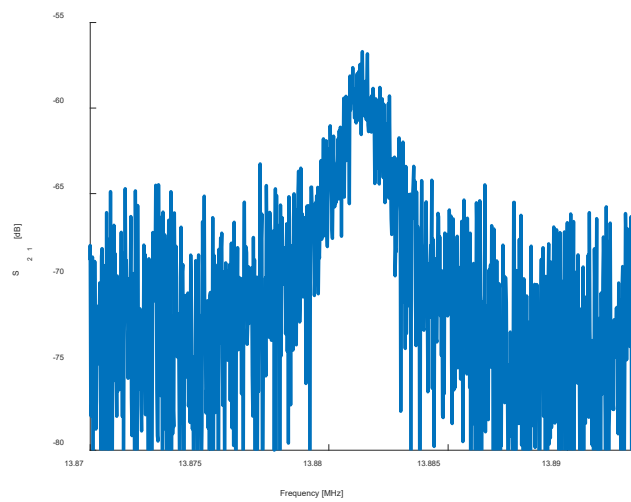


Figure 3.6. Measured frequency response for 13 MHz (C) device at  $V_p = 4.25V$ .

Equation (3.17) predicts that devices with lower stiffness, higher static capacitance, or smaller gaps will parametrically oscillate with a lower  $QV_pV_D$  product. The choices of devices in this work supports these claims. Device A was driven at two electrodes, while device B was driven at the disk. Consequently, equation (3.17) predicts that twice as much drive voltage is necessary for a given DC bias voltage and quality factor to excite device A compared to device B. The measured results support this with drive voltages for device A being approximately twice the drive voltages for device B. The slight discrepancy is due to non-equal quality factors. Device B has a slightly lower quality factor than device A, and thus requires more drive voltage to compensate, which the measured data also supports. Both devices B and C were driven at the disk, but differ in their gap size, stiffness, static capacitance, and quality factor. Device C has approximately 3/4 the gap, 1/3 the stiffness, 3 times the capacitance, and 1/5 the quality factor of device A. Consequently, equation (3.17) predicts that the necessary drive voltage of device C should be approximately 1/3 of device B. The measured results show that this back of the envelope calculation is fairly accurate.

### 3.3.3 Frequency Conditions

Prior works have demonstrated the existence stability regions for parametrically oscillating devices experimentally and through derivations using techniques such as Floquet's theorem and averaging [5] [3]. Regardless, the stability regions of Devices A, B, and C were measured to compare them to past work and to allow for comparison to future work.

Figure 3.7 shows the typical parametric oscillation frequency responses measured on the network analyzer. Note: the drive signal is twice the sense frequency. The stability regions are extracted from these measurements. Any response above the noise floor represents instability (oscillation). Notice that the forward and backward responses are different, which results in different stability regions for forward and backward sweeps.

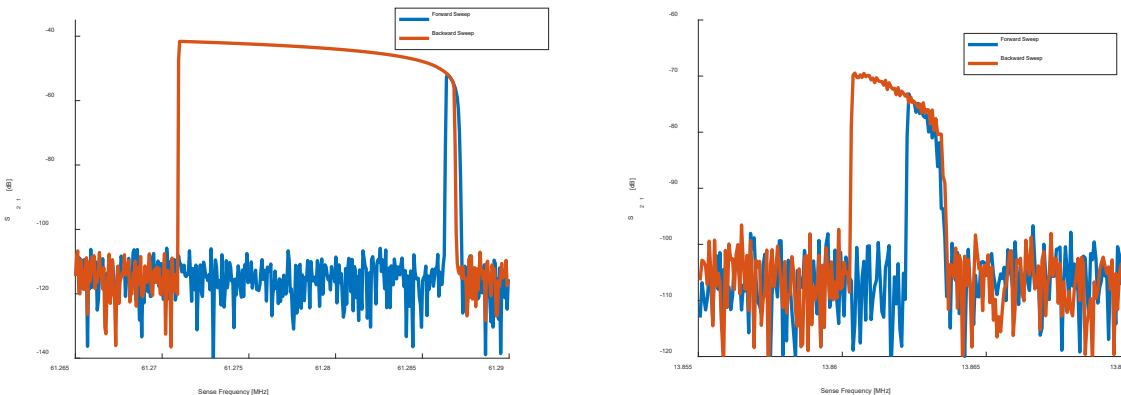


Figure 3.7. Typical measured parametric oscillation frequency responses for (Left) device B and (right) device C. The blue curve represents the forward (low frequency to high frequency) sweeps. The orange curve represents backward (high frequency to low frequency) sweeps.

Figure 3.8 shows the frequency stability regions with respect to the  $QV_pV_D$  product for device A. The parametric oscillation regions appear to be symmetric about the resonant frequency of the device for forward sweeps. However, the regions skew towards the lower frequencies for the backward sweeps.

Typically, the bandwidth for the forward sweeps is approximately  $\pm 0.0008\%$  from the resonant frequency. On the other hand, the bandwidths for the backwards sweeps are  $+0.0001\%/-0.05\%$  for backward sweeps. This suggests that these devices are not adequate for parametric filter applications unless the direction of the shift of the input frequency is adequately controlled [3]. For a given DC bias voltage, the bandwidth of the forward sweep seems to increase increasing drive voltage. However, this trend is not apparent in the backward sweep. In fact, the bandwidth of the backward sweeps appears to be more or less random.

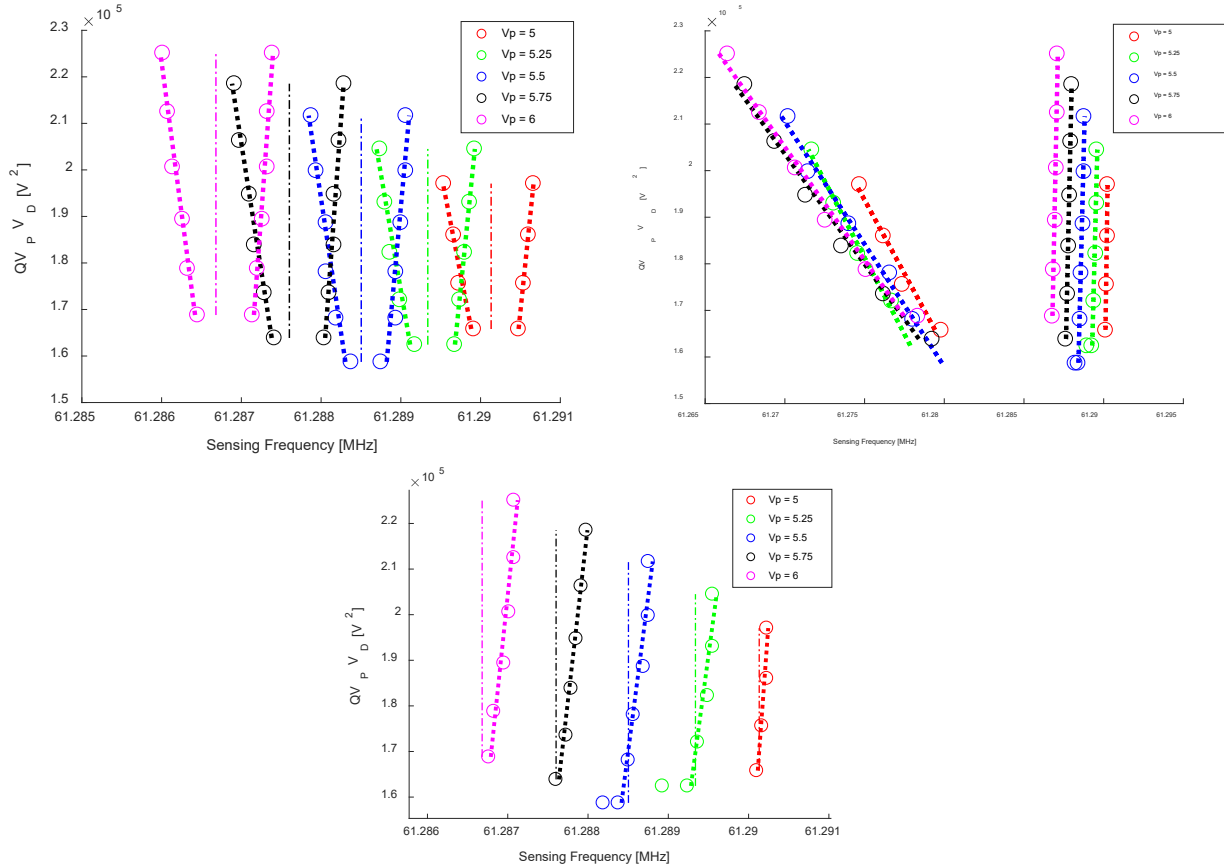


Figure 3.8. Stability regions for Device A with sweeping directions (Top Left) from low frequency to high frequency, (Top Right) high frequency to low frequency, and (bottom) high frequency to low frequency. The bottom graph is just the top right graph zoomed into the right four curves. The circles are the measured boundaries of oscillation for various DC bias voltages. The dotted lines are the linear best-fit lines used to outline the Arnold tongue. There is parametric oscillation inside these lines and no oscillation outside these lines for a given DC bias voltage. The dotted-dashed line shows the resonant frequency of the device at that specific DC bias voltage.

Figure 3.9 shows the frequency stability regions with respect to the  $QV_pV_D$  product for device B. Contrasting to device A, the parametric oscillation regions are not symmetric about the resonant frequency of the device for forward sweeps. Instead, the regions skew towards higher frequencies. The backward sweeps follow the same trends as the backward sweeps for device A. The forward sweeps have a bandwidth of  $+0.0007\%/-0.0003\%$  and the backward sweeps have a bandwidth of  $+0.0003\%/-0.02\%$ . Consequently, it seems as though the bandwidth for parametric oscillation is larger for device A compared to device B. In other words, if a wider bandwidth were necessary, driving from the electrodes would be beneficial. However, the tradeoff is that twice as much drive voltage is necessary.

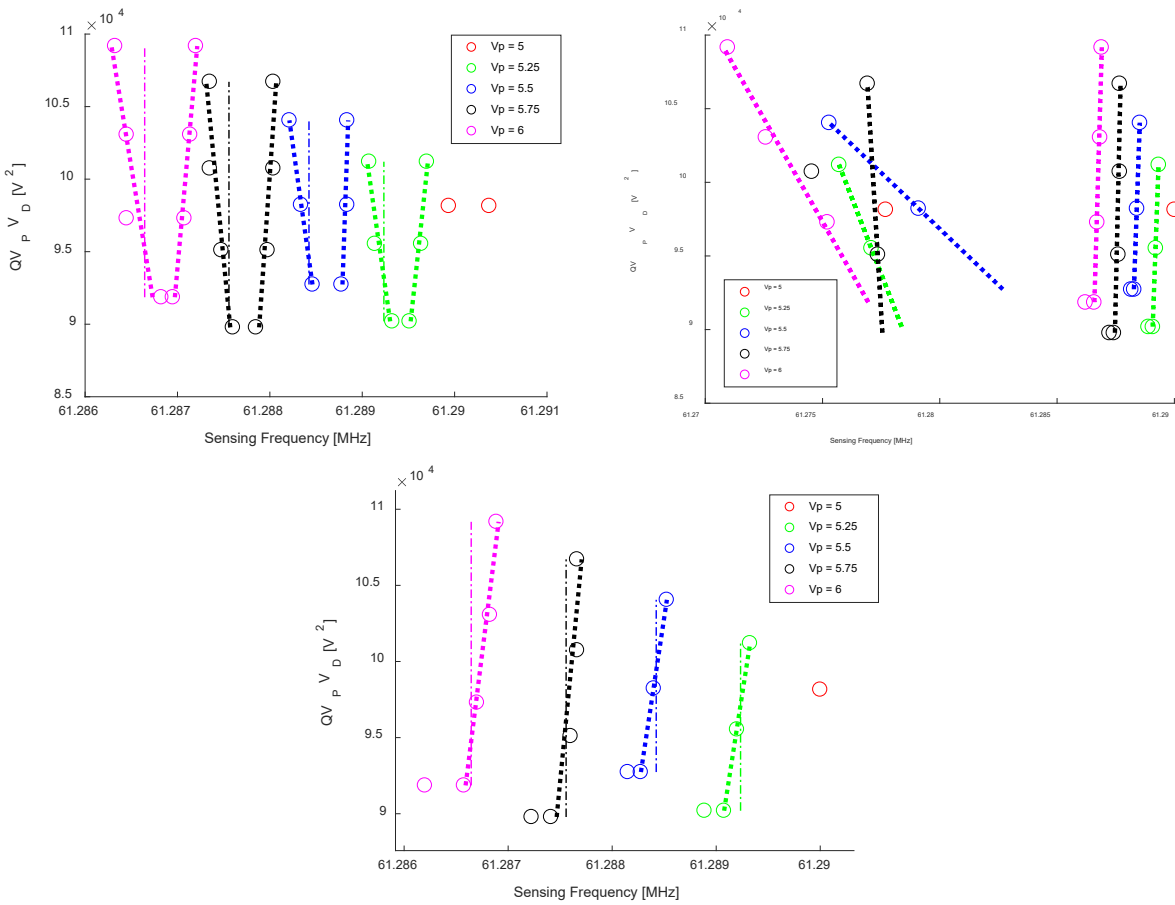


Figure 3.9. Stability regions for Device B with sweeping directions (Top Left) from low frequency to high frequency, (Top Right) high frequency to low frequency, and (bottom) high frequency to low frequency. These graphs are structured in the same way as Figure 3.8.

Figure 3.10 shows the frequency stability regions with respect to the  $QV_p V_D$  product for device C. Both the forward and backward sweeps are not symmetric about the resonant frequency. The forward sweeps skew towards high frequencies while the backward sweeps skew towards the lower frequencies. Another perspective is that these sweeps skew the regions such that the first frequency that causes parametric oscillation is close to the resonant frequency. The regions for the backward sweep for this device follows the same trend as the forward sweep regions, unlike devices A and B. This suggest that this design may be useful for parametric filtering applications. However, the bandwidth is still dependent on the sweep direction. The bandwidth of the forward sweep regions is approximately  $+0.008\%/-0.006\%$ , and the bandwidth of the backward sweep regions is  $+0.008\%/-0.01\%$ . The total bandwidths of the backward sweep regions are approximately twice the bandwidths of the forward sweep regions for given DC bias voltage and parametric drive voltage.

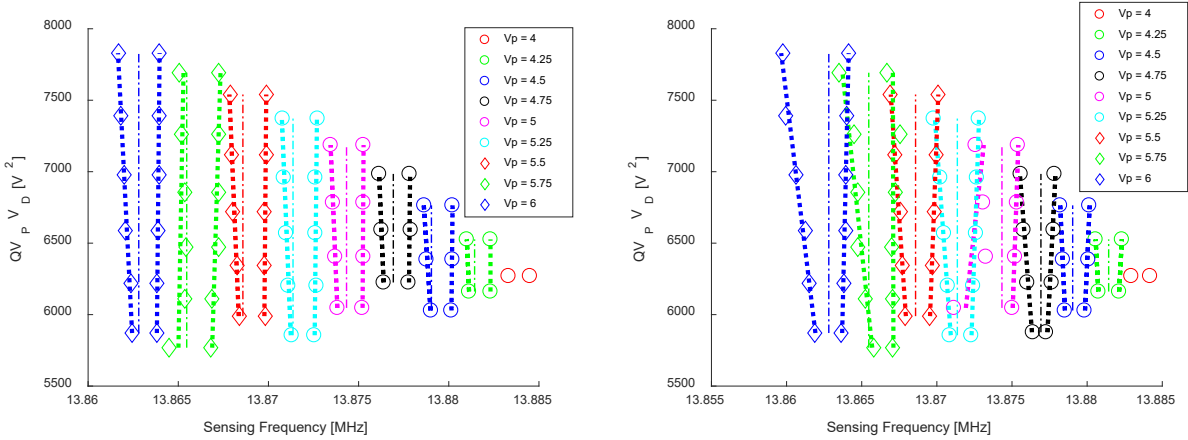


Figure 3.10. Stability regions for Device B with sweeping directions (Top Left) from low frequency to high frequency, (Top Right) high frequency to low frequency, and (bottom) high frequency to low frequency. These graphs are structured in the same way as Figure 3.8

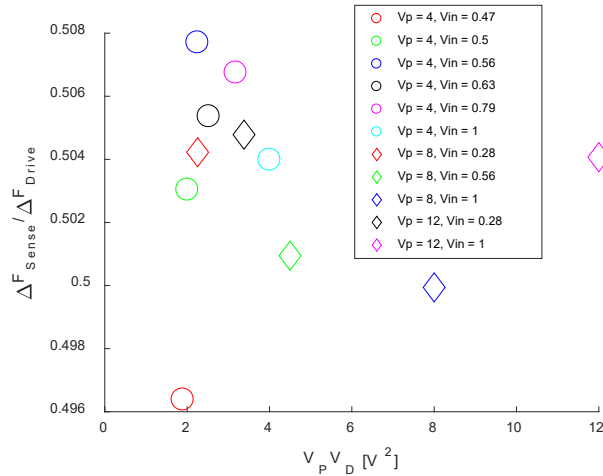


Figure 3.11. Measured changes in sense frequency due to changes in drive frequency as measured by the spectrum analyzer.

Figure 3.11 shows the change in sense frequency with change in drive frequency. The intent of this measurement is to support the prediction by equation (3.13) that the resulting frequency should track half of the parametric drive frequency. Figure 3.11 shows that this is precisely the case.

### 3.3.4 Stability and Safety

This section outlines the potential dangers of parametric oscillation. In fact, parametric oscillation can cause failures [5]. With the wineglass disk resonators, a particular failure mode is a drastic reduction in quality factor due to shorting. Notice that in Figure 3.7 that the parametric oscillation frequency responses slowly decrease towards higher frequencies for both forward and backward sweeps. A parametric frequency response that grows towards higher frequencies, as shown in Figure 3.12 (device D) and Figure 3.13 (device E), generally precedes the failure mode. Table 3.4 summarizes the changes in the frequency response due to shorting. Both shorting resonators experience shifts in frequency towards a high frequency, a decrease in quality factor, and increased noise in the measured  $S_{21}$ . The decrease in

quality factor was much more significant for the device E. This may be due to the very large initial quality factor of 107,150. Large quality factors imply that the size of motion is also large, which suggests that this disk may have slammed into the electrodes with much larger force causing a much larger degradation.

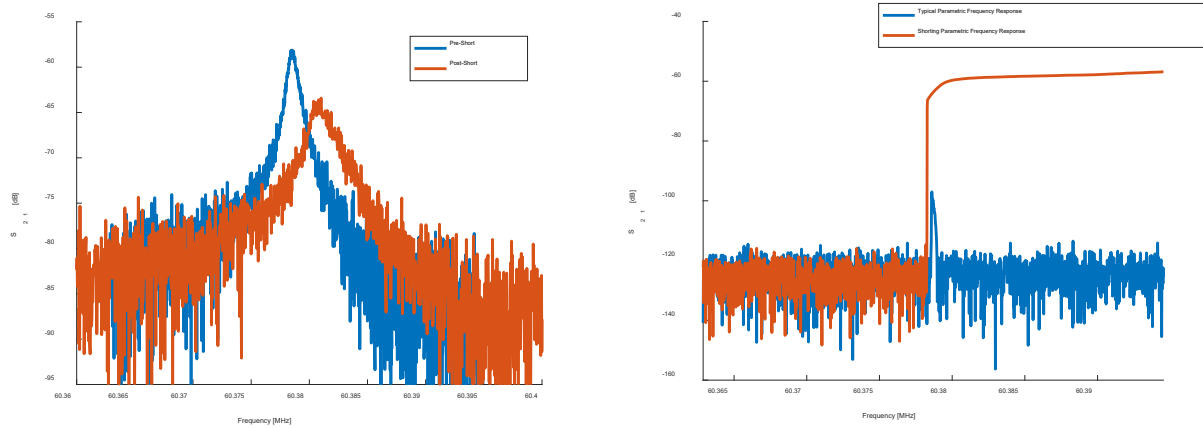


Figure 3.12. Measured (Left) frequency response and (Right) parametric oscillation response for Device D. The left figure shows the frequency response before and after failure. The right shows the parametric oscillation response that caused the failure. All responses were measured at 3V. The failure occurred when the parametric input power level was 6.8 dBm.

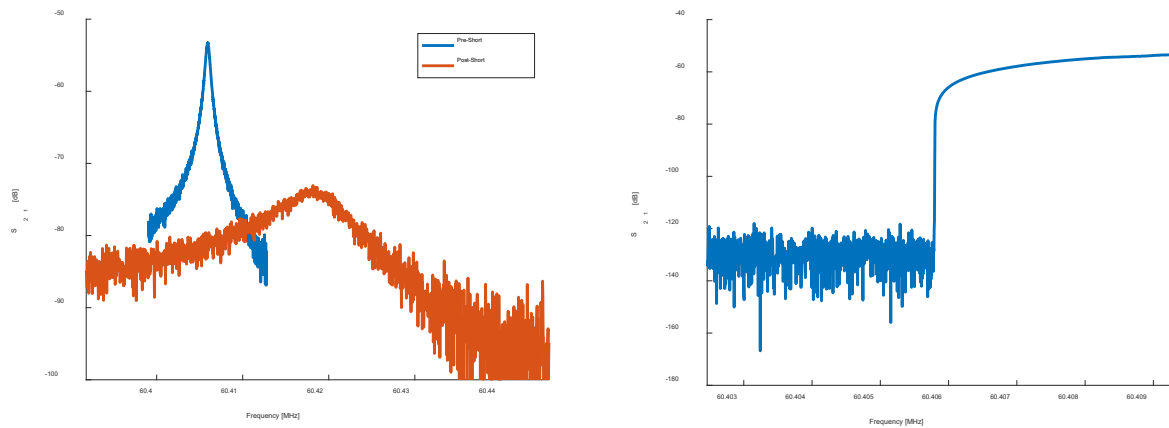


Figure 3.13. Measured (Left) frequency response and (Right) parametric oscillation response for Device E. The left figure shows the frequency response before and after failure. The right shows the parametric oscillation response that caused the failure. All responses were measured at 3V. The failure occurred when the parametric input power level was 1.5dBm.

Table 3.4. Summary of Device Failures for Devices D and E

	Device D		Device E	
	Pre-Short	Post-Short	Pre-Short	Post-Short
Resonant Frequency [MHz]	60.3785	60.3809	60.4059	60.4180
Quality Factor	64,747	40,373	107,150	12,343

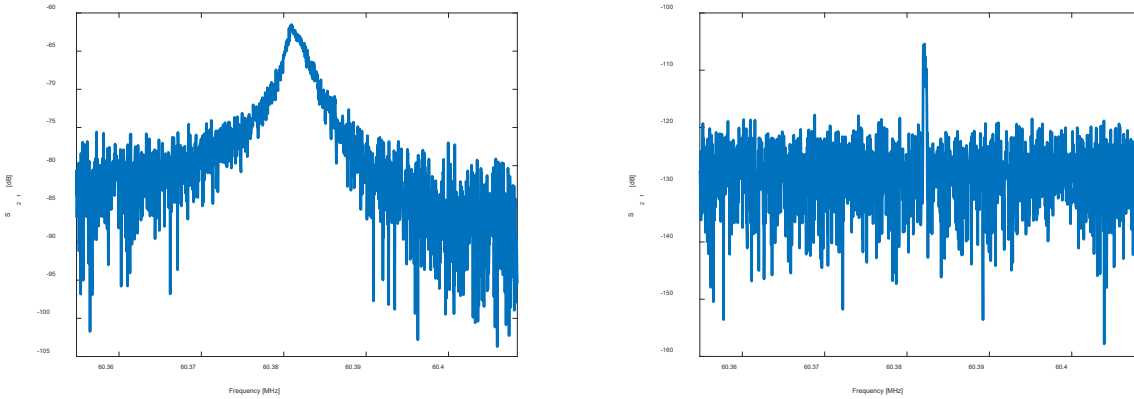


Figure 3.14. Measured (Left) frequency response of device D and (Right) parametric oscillation response at 3.75V. The input power was 9.8dBm. The measured quality factor was 32,467.

Interestingly, this failure mode does not necessarily stop the device from parametrically oscillating. Device D could still parametrically oscillate if given a large enough drive voltage, as shown by Figure 3.14.

Figure 3.15 demonstrates another interesting phenomenon of this failure mode. In general, wineglass disk resonators tend to have a negative electrical stiffness [4]. Consequently, as the DC bias voltage increases, the resonant frequency of the device should decrease. For device D, after the shorting failure, the device shows to have positive electrical stiffness. However, this phenomenon does not necessarily follow the failure mode discussed in this section. Device E, while it failed in the same way, still shows to have a negative electrical stiffness.

Despite these potentials for failures, parametric oscillation is safe if the parametric drive voltage is small enough. Devices A, B, and C did not experience failures due to limited drive voltage. Figure 3.16 shows the frequency response of device A before and after parametric oscillation. The change is negligible, and suggests that parametric oscillation can be a non-destructive technique.

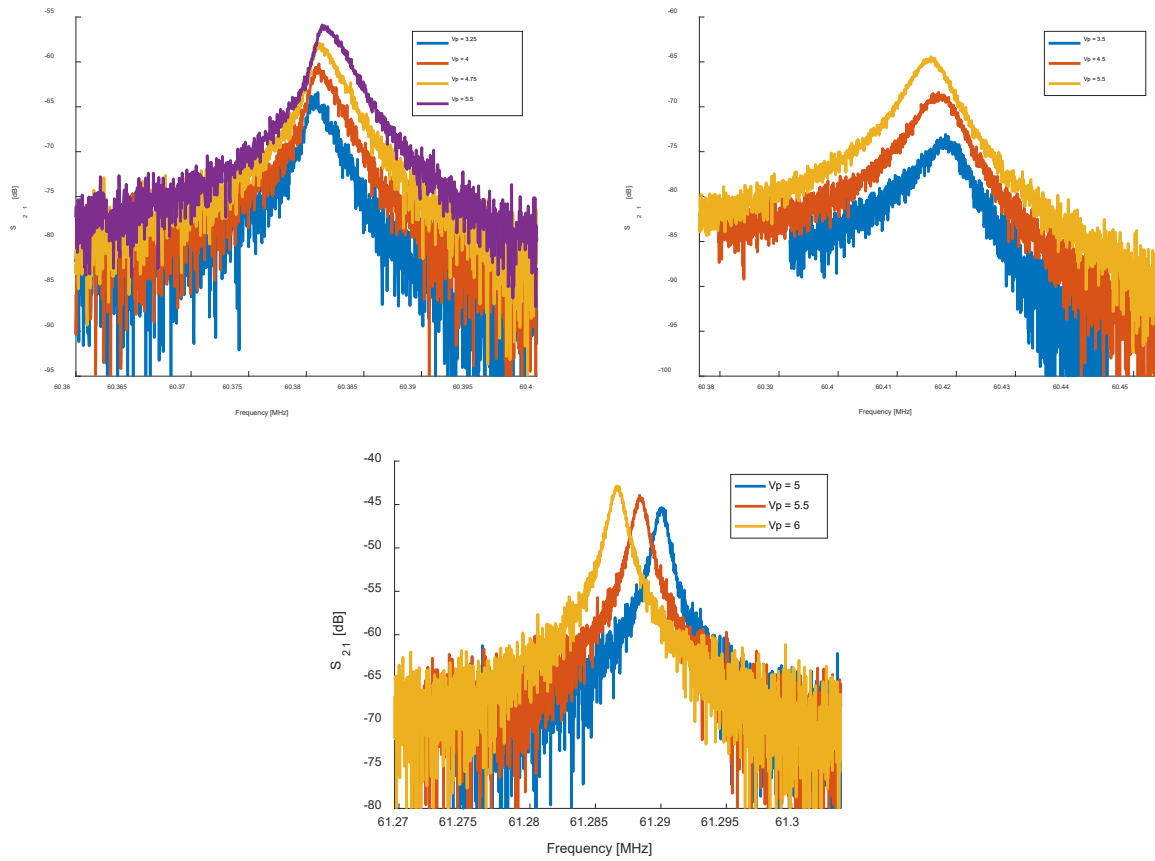


Figure 3.15 Measured frequency tuning of (Top Left) device D, (Top Right) device E, and (Bottom) device A. Device E and A show the expected negative electrical stiffness. Device D shows positive electrical stiffness.

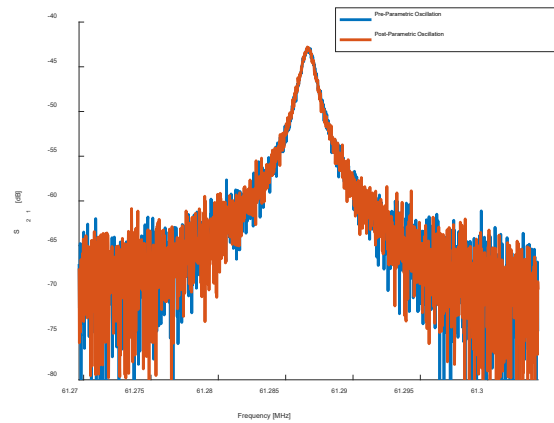


Figure 3.16. Measured frequency response of device A before and after parametric oscillation. The maximum input power was 0dBm at 6V.



## 4 CONCLUSION

---

### 4.1 RESULTS

This work derived voltage conditions for creating parametric oscillation for wineglass disk resonators. The result was a simple inequality that stated that the product of the drive voltage, quality factor, and DC bias voltage had to be larger than the product of various physical parameters of the resonator. The error between the lowest drive voltages necessary for given DC bias voltages differed by at most 16% across three different resonators. This work used two different resonator designs: 61MHz and 13MHz. Additionally, the parametric drive signal was applied to two different electrical positions: at the disk and on two electrodes. The parametric stiffness generated by this drive voltage is dependent on the number of electrodes that the signal is applied across. When the signal is applied to the disk, four electrodes create the electrical stiffness. When the signal was applied to two electrodes, only two electrodes create the electrical stiffness. Consequently, both the theory and the measurements show that approximately twice as much voltage is necessary to induce parametric oscillation for the two-electrode driven resonator over the disk driven resonator. The last resonator used demonstrated the effect of reducing the total stiffness of the device, the disk-to-electrode gap, and the disk-to-electrode capacitance on parametric oscillation conditions. Theoretical and experimental results show that decreasing stiffness, decreasing gap, and increasing capacitance decrease the voltage necessary for parametric oscillation at a given DC bias voltage.

This work also provided the measured frequency conditions for parametric oscillation. By sweeping the frequency of the input from low to high and high to low and measuring the output response, regions of instability were determined. Bandwidth of these regions were larger for the electrode driven resonators compared to the disk driven resonators. Across all three resonators, the forward sweeping instability regions shifted towards lower frequencies as the DC bias voltage was increased. The negative stiffness known to occur in capacitively transduced micromechanical resonators completely explains this effect. As the DC bias voltage increases, the resonant frequency decreases. Parametric oscillation occurs close to the resonant frequency, so shifts in the resonant frequency should correspond to translations of the instability regions. The bandwidths of the backwards sweeps appeared random for the 61MHz devices. However, the bandwidths of the 13MHz devices qualitatively were similar to the forward sweeping bandwidths, but differed in that the regions were slightly wider. In addition, measurements demonstrated that the output frequency of the parametric oscillation tracks half of the input drive frequency.

Finally, this work reports on a particular failure mode seen in various resonators. Under parametric oscillation, the device can potentially short and cause permanent damage to the device. Typically, the quality factor of the device would decrease, and the resonant frequency of the device would increase slight. However, if the decrease in quality factor is not too much, as with one of the devices present, the device can still parametric oscillate. Regardless, the shorting only occurs with high input powers with high quality factor devices. If the input power is limited, shorting does not occur and the device does not experience any compromising changes due to parametric oscillation.

## 4.2 FUTURE RESEARCH

This report achieved predicting the voltage conditions for parametric oscillation. In order to fully utilize parametric oscillation in wineglass disk resonator applications, more work is necessary in fully understanding this phenomenon. In particular, more effort can be placed on the following:

1. Develop theory on the shape of the instability regions for the wineglass disk resonator
2. Investigate the phase noise impacts of daisy-chaining multiple devices together through parametric oscillation
3. Investigate the phase impacts of daisy-chaining multiple devices through parametric oscillation for frequency synthesis purposes
4. Investigate the mechanisms for positive electrical stiffness due to failures caused by parametric oscillation

## 5 REFERENCES

---

- [1] Lord Rayleigh Sec. R. S., "XVII. On the maintenance of vibrations by forces of double frequency, and on the propagation of waves through a medium endowed with a periodic structure," *The London, Edinburgh, and Dublin Philosophical Magazine and Journal of Science*, pp. 145-159, 1887.
- [2] T. O. Rocheleau, R. Liu, J. N. Nilchi, T. L. Naing and C. T.-C. Nguyen, "A micromechanical parametric oscillator for frequency division and phase noise reduction," *2014 IEEE 27th International Conference on Micro Electro Mechanical Systems (MEMS)*, 2014.
- [3] B. DeMartini, J. Moehlis, K. Turner, J. Rhoads, S. Shaw and W. Zhang, "Modeling of parametrically excited microelectromechanical oscillator dynamics with application to filtering," in *SENSORS, 2005 IEEE*, 2005.
- [4] M. Akgul, L. Wu, Z. Ren and C. T.-C. Nguyen, "A negative-capacitance equivalent circuit model for parallel-plate capacitive-gap-transduced micromechanical resonators," *IEEE Transactions on Ultrasonics, Ferroelectrics, and Frequency Control*, vol. 61, no. 5, pp. 849-869, May 2014.
- [5] L. Moreno-Ahedo, R. Carmona, R. Francisco, F. Ortiz and I. Cruz, "On the implementation of a parametric oscillator in analog applications," in *2012 8th International Caribbean Conference on Devices, Circuits and Systems (ICCDACS)*, 2012.
- [6] A. Ozgurluk, M. Akgul and C. T.-C. Nguyen, "RF Channel-Select Micromechanical Disk Filters, Part I: Design," in *IEEE Transactions on Ultrasonics, Ferroelectrics, and Frequency Control*, 2018.
- [7] J. N. Nilchi, R. Liu and C. T.-C. Nguyen, "High Cx/Co 13nm-capacitive-gap transduced disk resonator," in *2017 IEEE 30th International Conference on Micro Electro Mechanical Systems (MEMS)*, 2017.
- [8] T. L. Naing, T. O. Rocheleau, E. Alon and C. T.-C. Nguyen, "A 78-microwatt GSM phase noise-compliant pierce oscillator referenced to a 61-MHz wine-glass disk resonator," in *2013 Joint European Frequency and Time Forum & International Frequency Control Symposium (EFTF/IFC)*, Prague, Czech Republic, 2013.
- [9] T. L. Naing, T. O. Rocheleau, Z. Ren, E. Alon and C. T.-C. Nguyen, "Vibration-insensitive 61-MHz micromechanical disk reference oscillator," in *2012 IEEE International Frequency Control Symposium Proceedings*, 2012.